Probabilistic Constrained Load Flow Considering Integration of Wind Power Generation and Electric Vehicles

John G. Vlachogiannis

***Abstract*—A new formulation and solution of probabilistic constrained load flow (PCLF) problem suitable for modern power systems with wind power generation and electric vehicles (EV) demand or supply is represented. The developed stochastic model of EV demand/supply and the wind power generation model are incorporated into load flow studies. In the resulted PCLF formulation, discrete and continuous control parameters are engaged. Therefore, a hybrid learning automata system (HLAS) is developed to find the optimal offline control settings over a whole planning period of power system. The process of HLAS is applied to a new introduced 14-busbar test system which comprises two wind turbine (WT) generators, one small power plant, and two EV-plug-in stations connected at two PQ buses. The results demonstrate the excellent performance of the HLAS for PCLF problem. New formulae to facilitate the optimal integration of WT generation in correlation with EV demand/supply into the electricity grids are also introduced, resulting in the first benchmark. Novel conclusions for EV portfolio management are drawn.**

***Index Terms*—Constrained load flow, correlation model, electric vehicles integration, planning period, stochastic learning automata, wind power penetration.**

I. Introduction

THE constrained load flow (CLF) problem deals with the adjustment of the power system control variables in order to satisfy physical and operating constraints. Therefore, a number of algorithms have been developed, based on modification of the Jacobian matrix formed in the standard load flow method using sensitivity or injection-changing-error feedback control [1], [2] or evolutionary computation techniques [3], [4]. The CLF problem is also expressed as a constrained optimization problem falling within the general class of optimal power flow (OPF) problems [5]–[8]. In most published methods, one or more known sets of generation and loads are assumed, i.e., the input variables are assumed deterministically known. These methods [1]–[8], however, are inefficient in providing offline settings of control variables that must remain optimal for a whole planning period. The problem of offline control settings has been tackled by the probabilistic CLF (PCFL) formulation [9], [10]. The method developed in [9] takes into account load uncertainties and generating unit unavailability modeled as probability density functions and provides control settings satisfying constraints over a whole planning period. Dispatching effects and topological variations are considered using probabilistic techniques. The control variable settings are based on sensitivity analysis of the constrained variables with respect to the control variables. Although this method has shown to provide settings satisfying the required constraints, it provides suboptimal solutions dependent on the initial values of the control settings. In [10], the problem is solved by means of reinforcement learning (RL) method. It is formulated as a multistage decision problem. Optimal control settings are learned by experience adjusting a closed-loop control rule, which is mapping states (load flow solutions) to control actions (offline control settings). The control settings are based on rewards, expressing how well actions work over the whole planning period, i.e., how well the operating limits of constrained variables are satisfied. In [11], the problem is solved by the implementation of ant colony system (ACS) method achieving better results than [10]. However, in all above studies, CLF problem reflects on conventional structure of the power systems.

In current open energy market environment, the high penetration of wind power into the power systems and the forthcoming introduction of electric vehicles (EV) into the transport system, the energy sector, mainly the electric power system, will suffer a dramatic change due to this important and expected issue. So, there is the need to develop new models, to facilitate the operation and optimal control of the new structure of the power systems. Therefore, in addition to conventional generation and load pattern considered in the PCLF problem, the wind power generation and EV demand/supply models are also included. In the state-of-the-art published material related to the forthcoming EV integration into the electric networks [12]–[19], there is only one EV demand model for load flow studies [19]. In [19], the charging process is developed based on queuing theory [20] and considering maximum capacity of plug-in EV at each load bus ($\mathrm{M}/\mathrm{M}/n_{\max}$ queue). So, it has limited applicability. In this paper, a new general model of EV for load flow studies is developed where the charging and discharging processes are considered. In this model, there is no limit in the capacity of plug-in EV at each load bus ($\mathrm{M}/\mathrm{M}/\infty$ queue [20]). Moreover, the wind power generation is included using a stochastic profile based on the wind velocity probability function [21]–[26].

The stochastic, nonlinear, nonconvex, nonsmoothness nature of the PCLF problem as well as the mixed type of control variables (continues and discrete) request the implementation of a hybrid stochastic optimization technique. A feasible and effective technique could be based on Learning Automata (LA) [27]–[40]. In recent years, LA have attracted the attention of scientists and technologists from a number of disciplines, and

Manuscript received December 10, 2008; revised March 02, 2009. First published September 25, 2009; current version published October 21, 2009. Paper no. TPWRS-00981-2008.

The author is with the Department of Electrical Engineering, Technical University of Denmark, Kgs. Lyngby DK-2800, Denmark (e-mail: iv@elektro.dtu.dk).

Digital Object Identifier 10.1109/TPWRS.2009.2030420

have been applied to a wide variety of practical problems in which *a priori* information is incomplete. In fact, observations measured from natural phenomena possess an inherent probabilistic structure [34]. The main advantages of LA over heuristic optimization and Monte Carlo techniques are: *1*) the LA guarantee a robust behavior without the complete knowledge of the stochastic and uncertain environment to be controlled (in contrast, Monte Carlo needs complete knowledge of the environment, that means large number of simulations and therefore large computational time); *2*) the action space of LA is not required to be a metric space as in Monte Carlo and heuristic techniques; *3*) the LA lead to global optimization, where in every stage, any element of the action set can be chosen, in contrast to heuristic techniques where the new value of the control variable has to be chosen close to the previous value; *4*) the contrast between Monte Carlo and LA is that LA learn more about which element causes good response with the highest probability according to the repeated procedure [36]; and *5*) LA uses a sigmoid multiobjective learning signal expressing the degree of satisfaction of the operating limits of all constrained variables in contrast to Monte Carlo, where the determination of the weighting factors among objectives is difficult [36]. Therefore, in this paper, a hybrid learning automata system (HLAS) is implemented to determine the optimal settings of discrete and continuous control variables involved in the PCLF problem. The implemented HLAS comprises new introduced reward-inaction continuous LA (R-CALA). Results are obtained on the introduced 14-busbar test system comprised by one small power plant (SPP), two WT generators, and two EV-plug-in stations connected at two PQ buses. In this system, three transformer taps with discrete positions, two shunt VAR compensation devices (one with continuous and one with discrete reactive power output), and a voltage magnitude are considered control variables. The results demonstrate the excellent performance of the proposed HLAS for the new formulation of PCLF problem.

In conclusion, the introduction of EV in correlation with high penetration of wind energy into the electricity grid is a unique opportunity to decrease oil, coal/fossil fuel dependency, CO_2 emissions from the transport sector, and achieving more flexible power pricing. This paper contributes clearly in the literature with: *1*) the new formulation of the PCLF problem incorporating wind power and EV stochastic profiles, *2*) implementation of HLAS for PCLF comprising new R-CALA components, *3*) development of general EV demand/supply model for load flow studies, *4*) introduction of new formulae facilitating the optimal incorporation of wind power in correlation with EV demand/supply into the electric networks and resulting in the first benchmark, and *5*) novel conclusions useful for EV portfolio management and vital importance in countries with high wind penetration are drawn.

II. Constrained Load Flow Problem

The CLF problem can be expressed by the two sets of nonlinear equations [10]:

$$\mathbf{Y} = \mathrm{g}(\mathbf{X}, \mathbf{U}) \tag{1}$$

$$\mathbf{Z} = \mathrm{h}(\mathbf{X}, \mathbf{U}) \tag{2}$$

where $\mathbf{Y}$ represents the nodal power injections vector; $\mathbf{Z}$ represents the constrained variables vector (power flows, reactive powers of PV buses, voltage at PQ buses, etc.); $\mathbf{X}$ represents the state vector (voltage angles and magnitudes); and $\mathbf{U}$ represents the control vector (transformer tap positions, shunt VAr compensations, voltage of PV buses, etc.)

The objective of constrained load flow is to maintain some or all the elements of $\mathbf{X}$ and $\mathbf{Z}$ vectors within given operating limits under stochastic generation and load variations. This can be achieved by selecting appropriate (robust) values of control variables $\mathbf{U}$ under random variations of loads and generations (noise factors) within their operating range [10].

III. Wind Power Generation for Load Flow Studies

The real power loss of a WT is estimated by the polynomial expression [24]

$$P_{loss} = a_p + b_p \cdot P_w + c_p \cdot P_w^2 \tag{3}$$

where the mechanical power output (P_w) is given by

$$P_w = \frac{\rho}{2} \cdot C_p \cdot \pi \cdot R^2 \cdot V_w^3. \tag{4}$$

The power coefficient (C_p) is a nonlinear function of the tip speed ratio λ and the pitch angle ϑ given by [21]:

$$C_p = 0.5 \cdot \left(\frac{116}{\Lambda} - 0.4 \cdot \vartheta - 5 \right) \cdot e^{\frac{-21}{\Lambda}} \tag{5}$$

where

$$\frac{1}{\Lambda} = \frac{1}{\lambda + 0.08 \cdot \vartheta} - \frac{0.035}{\vartheta^3 + 1}. \tag{6}$$

The real power output of WT is given by

$$P_g = P_w - P_{loss} = -a_p + (1 - b_p) \cdot P_w - c_p \cdot P_w^2. \tag{7}$$

The air density (ρ), blade radius (R), blade pitch angle (ϑ), tip speed ratio (λ), power loss coefficients (a_p, b_p, c_p), cut-in, and cut-out wind speed velocity are given in Section VI. The wind velocity (V_w) follows the Weibull distribution [26]:

$$f(V_w) = \frac{\kappa}{\mu} \cdot \left(\frac{V_w}{\mu} \right)^{k-1} \cdot e^{-\left(\frac{V_w}{\mu}\right)^k}. \tag{8}$$

In the programming code of load flow, values of wind velocity (8) are iteratively calculated using the following formula [41]:

$$V_w = \mu \cdot (-\ln(1 - r))^{\frac{1}{k}} \tag{9}$$

where r is random variable uniformly distributed. The shape (κ) and scale (μ) factors define the wind profile and given in Section VI.

Considering constant power factor of the WT, the Q-limits enforced in the generator during the load flow calculations are given by [25]

$$Q_{\max} = \pm \frac{P_g}{P_w} \cdot \sqrt{S_N^2 - P_w^2}. \tag{10}$$

Using (7), the Q-limits are obtained as

$$Q_{\max} = \pm \left[-a_p + (1 - b_p) \cdot P_w - c_p \cdot P_w^2\right] \cdot \sqrt{\frac{S_N^2}{P_w^2} - 1}. \tag{11}$$

During the load flow process, the WT generator's voltage output is considered constant at the nominal value (1 p.u.).

IV. EV Demand/Supply Model for Load Flow Studies

The charging and discharging process of EV at each load bus are developed based on probabilistic models of statistics.

From the open literature, it is well known that all battery systems of EV are chemical storage devices and their charge/discharge modus operandi are chemical processes. So, they are exponential functions over time. Specifically, the instantaneous charging status of the battery system of EV is simulated by the following exponential formula [19]:

$$P_{EV}(t) = P_{EV,\max} \cdot (1 - e^{-\alpha \cdot t/t_{\max}}) + P_{EV,0} \tag{12}$$

where the current status of the battery system is $P_{EV,0}$; the maximum power capacity of EV is $P_{EV,\max}$; and the maximum charging time is $t_{\max}$. Similarly, the instantaneous discharging status of the battery system of EV is simulated by the following exponential formula:

$$P_{EV}(t) = P_{EV,0} \cdot e^{-\alpha \cdot t/t_{\max}}. \tag{13}$$

The constant parameter α can be calculated assuming that a fully empty battery system of EV absorbs 97% of maximum power capacity approximately in the third part of the maximum charging time, $t_{\max}/3$. This is a general assumption for most of the modern battery systems.

Full charge: Assuming that if a plug-in EV needs t_d hours to be fully charged, then using (12), the active power demand from the network is given by

$$P_{EV,\mathrm{dem}} = P_{EV,\max} \cdot (1 - e^{-\alpha \cdot t_d/t_{\max}}). \tag{14}$$

Full discharge: Assuming that if a plug-in EV needs $t_s = t_{\max} - t_d$, hours to be fully discharged, then using (13), the active power injection into the network is given by

$$P_{EV,\mathrm{supply}} = P_{EV,\max} \cdot e^{-\alpha} \cdot e^{\alpha \cdot t_s/t_{\max}}. \tag{15}$$

The active power demand/supply from/into the network (14) and (15) is restricted only by the charging/discharging rate capability of each EV battery system [18].

A. EV-Plug-In System

Using (14) and (15), each load bus supports a system of n plug-in EV with total active power (difference between active power demand and injected power into the network) given by

$$P_{EV,total} = P_{EV,\max} \cdot \left(n_d - \sum_{i=1}^{n_d} e^{-a \cdot t_{di}/t_{\max}} - e^{-a} \cdot \sum_{i=1}^{n_s} e^{a \cdot t_{si}/t_{\max}} \right). \tag{16}$$

Integrating (14) and (15) for a system of n plug-in EV, the total energy demand/supply is obtained as

$$E_{EV,total} = \frac{P_{EV,\max} \cdot t_{\max}}{\alpha} \cdot \left[\sum_{i=1}^{n_d} \left(\frac{\alpha \cdot t_{di}}{t_{\max}} + e^{-a \cdot t_{di}/t_{\max}} \right) - n_d - e^{-a} \cdot \left(\sum_{i=1}^{n_s} e^{a \cdot t_{si}/t_{\max}} - n_s \right) \right] \tag{17}$$

where $n_d + n_s = n$.

A portion of plug-in EV is considered as charged EV (n_d) and the rest as discharged ones (n_s). The mean portion of discharged EV (n_s) over all plug-in EV, the expected number of plug-in EV (λ) and the mean service time (t_μ) at each load bus will be derived from measurements on a real system. Since there is no such system at the moment, in this paper, they are considered as predefined parameters.

In terms of queuing theory, charged/discharged EV are considered as customers to be served in $\mathrm{M/M/\infty}$ queue [20]. As queuing theory mandates, the number of charged/discharged EV follows Poisson distribution and their service time follows the exponential distribution [19], [20]. Specifically, the number (n) of plug-in EV at each load bus in a fixed period of time (e.g., in an iteration of load flow process) follows the following distribution:

$$p(n) = \frac{e^{-\lambda} \cdot \lambda^n}{n!}, \quad n = 0, 1, \ldots \tag{18}$$

where λ is a positive real number, equal to the expected number of plug-in EV in an iteration of load flow.

In the programming code of load flow, the number (n) of plug-in EV at each load bus (18) is iteratively calculated using the Knuth algorithm [42].

The service time $(t_{service})$ for each EV [time to be fully charged (t_d) or fully discharged (t_s)] follows the exponential possibility distribution. If the mean of service time is t_μ, then the probability is given by

$$p(t_{service}) = \frac{e^{-t_{service}/t_\mu}}{t_\mu}. \tag{19}$$

In the programming code of load flow, the service time of each plug-in EV $(t_{service,i})$ (19) is iteratively calculated using the following formula:

$$t_{service,i} = \begin{cases} -t_\mu \cdot \ln(r), & \text{if } r \geq e^{-t_{\max}/t_\mu} \\ t_{\max}, & \text{else} \end{cases} \tag{20}$$

where r is random variable uniformly distributed.

Finally, considering unity constant power factor of the battery systems, the reactive power demand/supply of plug-in EV is equal to zero.

B. Regular Load

All other types of demand are considered as regular load following the same probability density function. Hence, a single distribution can be used for this real/reactive demand at each load bus [43]. The probability density function of the real/reactive power load can be either derived from measurements or assumed to be under the normal distribution $N(\mu, \sigma)$. In the programming code of load flow, real/reactive power load at each PQ bus is iteratively generated using the following formula:

$$X = \mu + \sqrt{2} \cdot \sigma \cdot \mathrm{erf}^{-1}(2r - 1) \tag{21}$$

where r is random variable uniformly distributed; erf^{-1} is the inverse error function; mean values μ are those given as fixed ones in the data of the system; and σ is the standard deviation.

V. HLAS for PCLF Problem

There is a strong and growing interest within the engineering community in the use of efficient optimization techniques for several purposes. Optimization techniques are commonly used as a framework for the formulation and solution of design problems. For example, in the context of control, the objective of an online optimization scheme is to track the real process optimum as it changes with time. This must be achieved without the process constraints to be violated.

In this paper, an LA-based system is implemented to solve the PCLF problem in modern power systems with stochastic wind power generation and EV demand/supply. Since the problem involves discrete and continues control variables, there is the need of implementation of an HLAS. The basic components of HLAS are represented in the next two subsections. In general, LA are divided into two main groups: finite action-set learning automata (FALA) and continuous action-set learning automata (CALA) based on whether the action set is finite or continuous.

A. S-Model Finite Actions Learning Automata (S-FALA)

FALA has finite number of actions and has been studied extensively. For an r-action FALA $\alpha_i, i = 1, 2, \ldots r$, the action probability distribution is represented by an r-dimensional probability vector $\mathbf{p}(n)$ at instant-n that is updated by the learning algorithm. The S-model of FALA (or S-FALA) is the FALA whose response takes continuous values over the unit interval [0, 1]. The response $\beta(n)$ at instant-n in the S-FALA means the degree of unfavorableness, which approaches 0 if the response is favorable and approaches 1 if the response is unfavorable [36]. The chronological sequence of probability vectors $\{\mathbf{p}(n)\}$ is a discrete-time Markov process on a suitable state space. A general linear reinforcement learning scheme in S-FALA for updating action probabilities is represented as follows.

If an action $\alpha_i, i = 1, 2, \ldots r$ at instant-n is chosen $(\alpha(n) = \alpha_i)$, then its probability is updated by

$$p_i(n+1) = p_i(n) - c_P \cdot \beta(n) \cdot p_i(n) + c_R \cdot (1 - \beta(n)) \cdot (1 - p_i(n)) \tag{22}$$

and the probabilities of other actions $j \neq i$ at the same instant-n are updated using

$$p_j(n+1) = p_j(n) + c_P \cdot \beta(n) \cdot \left(\frac{1}{r-1} - p_j(n) \right) - c_R \cdot (1 - \beta(n)) \cdot p_j(n). \tag{23}$$

In (22), the probability of taking an action α_i is increased if the response corresponding to this action is favorable [$\beta(n)$ is close to 0] and otherwise is decreased [$\beta(n)$ is close to 1]. In (23), the probability of taking other actions α_j, $j \neq i$ is increased if the response corresponding to chosen action α_i is unfavorable and otherwise is decreased. The penalty and reward parameters in (22) and (23) are denoted, respectively, by c_P and c_R defined over the interval [0, 1]. The above linear reinforcement-based S-FALA scheme for $c_P = c_R$, $c_P < c_R$, and $c_P = 0$ are called, respectively, the linear reward-penalty $(\mathrm{S} - \mathrm{FALA}_{R-P})$ scheme, the linear reward ε-penalty $(\mathrm{S} - \mathrm{FALA}_{R-eP})$ scheme, and the linear reward-inaction $(\mathrm{S} - \mathrm{FALA}_{R-I})$ scheme [36].

B. Continuous Actions Learning Automata (CALA)

In many applications, we have a large number of discrete actions or continuous actions. However, the S-FALA with too large number of actions converges slowly. In such applications, CALA, whose actions are chosen from real line, is very useful. In the literature, there are four CALA schemes [37]–[40]. In this paper, a new R-CALA is introduced. In the introduced R-CALA, the action probability distribution is represented by normal distribution function with mean $\mu(n)$ and standard deviation $\sigma(n)$. At each instant-n, the mean and standard deviation are updated by reinforcement learning signal $\beta(n) \in [0, 1]$ emitted by the environment. Specifically, the interaction between R-CALA and the random environment takes place as iterations by the following process: Instant-n begins by selection of an action $\alpha(n)$. This action is generated as a random variable from the normal distribution function with mean $\mu(n)$ and standard deviation $\sigma(n)$. The selected action $\alpha(n)$ is applied to the random environment and R-CALA receives an evaluated signal $\beta(n) \in [0, 1]$, from the environment. Then, the R-CALA updates the parameters $\mu(n)$ and $\sigma(n)$ using the following simple rules:

$$\mu(n+1) = \begin{cases} \alpha(n) & \text{if } \beta(n) < \beta_{\min} \\ \mu(n) & \text{else} \end{cases} \tag{24}$$

$$\sigma(n+1) = \sqrt[3]{\frac{a_{\max} - a_{\min}}{6 \cdot (n+1)}} \tag{25}$$

where a_{max}, a_{min} are the limits of action; $\beta_{\min}$ is the minimum value of reinforcement learning signal it ever encountered until instant $n - 1$.

The main advantage of the new simplified R-CALA is that no parameters need to be regulated, and therefore, it is very adaptable and sensitive to highly stochastic environments.

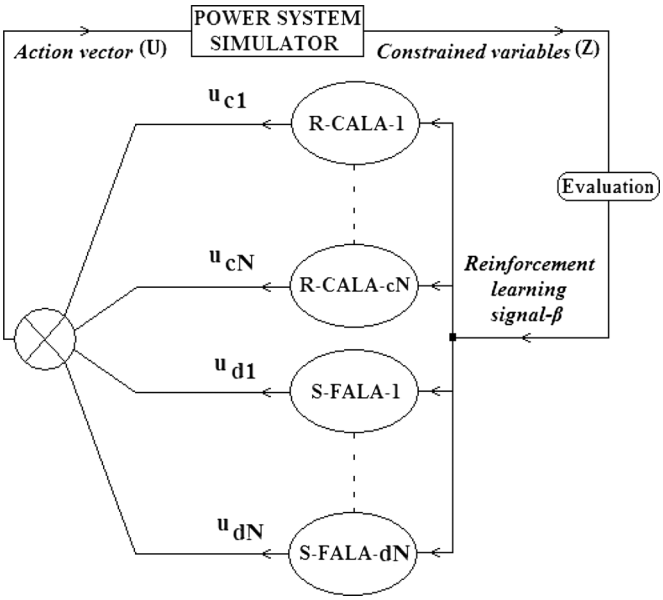

Fig. 1. Architecture of HLAS for probabilistic CLF problem.

C. Hybrid Learning Automata System (HLAS)

As previously mentioned, the PCLF problem involves discrete and continuous control variables. Therefore, S-FALA and R-CALA are interconnected in the architecture showed in Fig. 1, where cN and dN are the number of continuous and discrete control parameters, respectively. In general, the HLAS is a stochastic learning system comprising continuous (R-CALA) and discrete (S-FALA) LA (components) to find optimal settings of continuous and discrete control variables, respectively. It is a robust system since it can find very fast optimal solutions in a large stochastic and partially observed environment. At each instant, HLAS receives an operating point (state) of the environment as input and estimates a sigmoid reinforcement learning signal (multiobjective function). As output, control settings are determined by HLAS components enforced in the stochastic environment. The stochastic environment receives these actions responding a new operating point (state) and so on. Briefly, optimal control settings are learned by HLAS adjusting a closed-loop control rule, which maps states to control actions so as the reinforcement learning signal received by HLAS to be minimized. Specifically, the HLAS for PCLF proceeds as follows.

Step 1) A random operating point comprised by: *1*) pattern of regular load using (21), *2*) pattern of EV demand/supply [using (16), Knuth algorithm, (20)], *3*) pattern of wind power generation [using (7), (9)], and *4*) set of control actions [using (22), (23) for S-FALA and (24), (25) for R-CALA] is generated.

Step 2) A load flow is executed in power system's simulator and a reinforcement learning signal $\beta(n) \in [0,1]$ is calculated. This expresses the degree of satisfaction of the operating limits of all constrained variables. The appropriate reinforcement learning signal for the PCLF problem is introduced in the following subsection.

Step 3) All components of HLAS receive the same reinforcement learning signal $\beta(n)$. According to $\beta(n)$, each component updates its own action probability [(22), (23) for S-FALA and (24), (25) for R-CALA].

Step 4) Steps 1–3 are repeated until the reinforcement learning signal $\beta(n)$ is fixed in a minimum value or the maximum number of iterations is achieved (15 000 in this study).

Step 5) After iterative process, each S-FALA and R-CALA of HLAS adopts as optimal control action over the whole planning period the action that has the highest probability. The whole planning period is delimited by: *1*) the upper and lower values of regular and EV load demand and *2*) lower and upper values of WT real power generation, respectively.

D. Reinforcement Learning Signal

Application of the HLAS procedure in PCLF problem is linked to the choice of an appropriate reinforcement learning signal so that its value to be minimized while the limits of the constrained variables are satisfied for the whole planning period. An enforced empirical strategy is to consider the variations of constrained variables close to the means of their operating intervals as a measure for the reinforcement learning signal. So, it is computed by the average of all constrained variables at iteration-n, normalized in the interval: [0, 1], as follows:

$$\beta(n) = 1 - \frac{1}{k} \cdot \sum_{j=1}^{k} e^{-\left| \frac{2 \cdot Z_j(n) - Z_{j\max} - Z_{j\min}}{2} \right|} \qquad (26)$$

where k is the number of constrained variables and Z_j is the value of j-constrained variable bounded by lower $(Z_{j\min})$ and upper $(Z_{j\max})$ limit.

So, in terms of machine learning, $\beta(n)$ (26) is an immediate reward which determines if the limits of all constrained variables are satisfied.

VI. Results

A. PCLF Solution

The above described HLAS procedure is applied to CLF problem on the introduced 14-busbar test system (Fig. 2).

The 14-busbar test system is developed based on the standard IEEE 14-bus system and consists of the slack bus (node 1), four PV buses (nodes 2, 6, 7, and 10), ten PQ buses, and 18 branches. The characteristics of lines are kept similar to those given in the standard IEEE 14-bus system [44]. The available reactive power of capacitor connected at bus-3 is [0, 30] MVAr and the discrete values of reactive power of capacitor banks connected at bus-14 are {0, 3, 6, 9, 12, 15, 18, 21, 24, 27, 30} MVAr. The capacitors at buses 6 and 10 are fixed at value of 15 MVAr. Also, a fixed network topology is assumed. The regular load at nodes 2–6, 9, 10, and 12–14 follow normal distribution with mean values of those given as nominal ones in Appendix and standard deviation of 4%. The total installed capacity in the system is equal to 465 MW. In the introduced test system, two large power plants are connected at nodes 1 and 2, two WT-2 MW connected at

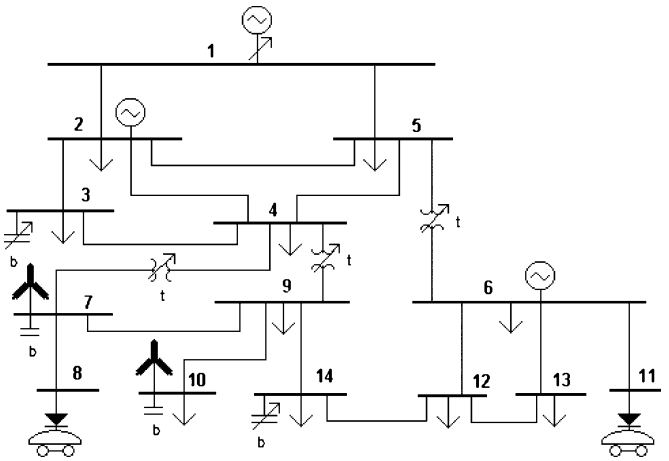

Fig. 2. One-line diagram of 14-busbar test system.

nodes 7 and 10, an SPP (10 MW) connected at node 6, and two EV-plug-in stations connected at nodes 8 and 11. The architecture of this system is useful for further research of EV demand/supply in direct relation with wind power generation (nodes 7 and 8) as well as in relation with other small energy sources (nodes 6 and 11).

In this study, the following parameters of WT are considered: mechanical power $P_w = 2$ MW; apparent electric power $S_N = 2.2$ MVA; air density $\rho = 1.225\ \mathrm{kg/m^3}$; blade radius $R = 30.6$ m; tip speed ratio $\lambda = 8$; pitch angle $\vartheta = 0°$; real power loss coefficients: $a_p = 40$ kW, $b_p = 0.01852$, and $c_p = 0.00001715\ \mathrm{kW^{-1}}$; cut-in and cut-out wind speed: 5 m/sec and 25 m/sec, respectively; shape and scale factor: $\kappa = 2$ and $\mu = 15$, respectively. It is important to note that the wind profile is not unique, as there is an infinite number of wind profiles that could be used [21], [22]. In this study, the specific model of Tesla Roadster EV is used [45]. A full charge of the battery system of Tesla Roadster EV requires $t_{\max} = 3.5$ h using the high power connector which supplies 70 A, 240 V electricity [45]. So, the maximum power capacity is $P_{EV,\max} = 70\ \mathrm{A} \times 240\ \mathrm{V} = 16.8\ \mathrm{kW}$ and the constant parameter α is calculated at a value of 10.137525. Using the developed formula (17), a full charged Tesla Roadster EV stores 53 kWh of electrical energy; the same value is reported in the technical specs of Tesla Roadster [45]. The battery system's charging and discharging rate capabilities of Tesla Roadster EV are not given in [45], and therefore, they are not considered in this study. The mean portion of discharged EV over all plug-in EV at nodes 8 and 11 is set at a value of 20% and 25%, respectively. The expected number of plug-in EV at nodes 8 and 11 is set at a value of 120 and 125, respectively. The mean service time of plug-in EV at both nodes is considered at 2.5 h.

The control variables of PCLF comprise all transformer taps (t_{56}, t_{49}, t_{47}) discretized at 16 positions in the range of [0.9, 1.05], continuous reactive power compensation at bus 3 (b_3), discrete capacitor banks connected at bus 14 (b_{14}), and voltage magnitude of slack bus-1 in the range of [0.96, 1.04] p.u. (Fig. 2). Specifically, the upper part of Table I shows the limits of all control variables. In the lower part of Table I, the upper and lower limits of all constrained variables are shown.

TABLE I
LIMITS OF CONTROL AND CONSTRAINED VARIABLES OF 14-BUSBAR TEST SYSTEM

Control actions	*Umin*	*Umax*
t_{56}	0.90	1.05
t_{49}	0.90	1.05
t_{47}	0.90	1.05
b_3	0.00	0.30
b_{14}	0.00	0.30
V_1	0.96	1.04
Constrained variables	*Zmin*	*Zmax*
Q_{g2}	0.00	0.40
Q_{g6}	0.00	0.03
Q_{g7}	-0.018	0.018
Q_{g10}	-0.018	0.018
S_{23}	0.00	0.75
S_{56}	0.00	0.35
V_3	0.96	1.05
V_4	0.96	1.05
V_5	0.96	1.05
V_8	0.96	1.05
V_9	0.96	1.05
V_{11}	0.96	1.05
V_{12}	0.96	1.05
V_{13}	0.96	1.05
V_{14}	0.96	1.05

These include reactive powers (Q_{gi}) at generation buses 2, 6, 7, and 10; apparent power flows (S_{ij}) in the lines 2–3 and 5–6; and voltages at load buses (V_i).

Table II gives the optimal reinforcement learning signal, the optimal control actions, and the operating space of constrained variables when the greedy-optimal action is enforced over the whole planning period. After HLAS process, the optimal reinforcement learning signal emitted by the stochastic environment is 0.01366 and achieved rapidly after 329 iterations (Fig. 3). Since the initial value of reinforcement learning signal is 0.04917, HLAS achieves a significant control efficiency of 72.22%. From Table II, it can be seen that even when applying the greedy-optimal control settings, reactive production at node 6 (Q_{g6}) violates its upper limit. In Table II, these results are also compared with the base case where nominal values of control actions are enforced over the whole planning period.

It can be seen that the HLAS provides improved results, since the limits of reactive production at nodes 2 and 7, lower and upper limit of reactive production at node 6 and node 10, respectively, upper limit of the apparent power flow in line 5–6, and lower limits of voltages at nodes 3 and 4 are not violated. However, the violation of upper limit of reactive production at SPP (Q_{g6}) is due to the increased reactive demands of the system and the available control actions cannot enforce the violated limit. One way of enforcing violated limit is to relax the constant voltage limitation at node 6 and allowing the voltages at nodes 2 and 10 to be set at higher values.

B. Integration of Wind Power in Correlation With Electric Vehicles into Electricity Grids

Motivated by a recent research dealing with impact of wind power variations on the operation of power systems considering load dynamics [46], here, a benchmark for optimal integration of wind power in association with EV into the steady-state operation of power systems is set up. New formulae to facilitate

TABLE II
PCLF RESULTS OF HLAS ON 14-BUSBAR TEST SYSTEM

HSLA			Base Case	
$\beta = 0.01366$			-	
Actions	Greedy-Optimal Settings		Nominal Settings	
t56	1.00		0.932	
t49	1.04		0.969	
t47	1.00		0.978	
b3	0.30		0.075	
b14	0.30		0.060	
V1	1.00112		1.01	
Constrained Variables	*Zmin*	*Zmax*	*Zmin*	*Zmax*
Q_{g2}	0.17540	0.34386	0.42091*	0.55096*
Q_{g6}	0.02897	0.11892*	-0.05186*	-0.02104*
Q_{g7}	0.00000	0.00000	0.02751*	0.06410*
Q_{g10}	0.00000	0.00000	0.01176	0.03505*
S_{23}	0.64894	0.70549	0.64937	0.71284
S_{56}	0.27088	0.32524	0.31221	0.35203*
V_3	0.97271	0.98104	0.94099*	0.94754*
V_4	0.97716	0.98452	0.95829*	0.96243
V_5	0.98166	0.98723	0.96340	0.96693
V_8	0.99175	1.00373	0.99999	1.00000
V_9	0.98504	0.99884	0.98881	0.99022
V_{11}	0.99819	0.99999	0.99783	1.00000
V_{12}	0.99449	1.00099	0.97756	0.98003
V_{13}	0.97699	0.97880	0.97698	0.97881
V_{14}	1.01024	1.02369	0.96950	0.97350

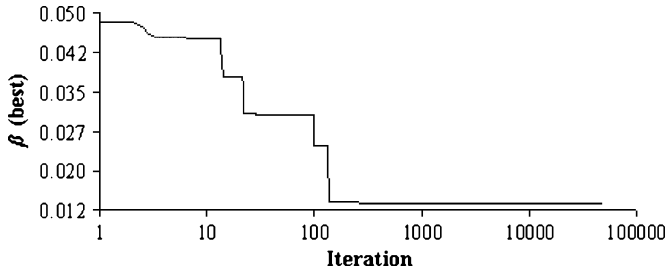

Fig. 3. Evolution of best value of reinforcement learning signal (logarithmic scale of iteration numbers).

TABLE III
STATISTICAL ANALYSIS FOR WT GENERATION AND EV DEMAND OF 14-BUSBAR TEST SYSTEM

Component	Mean (MW)	Standard deviation
WT-2MW (node 7)	1.0918	0.8360
EV-station (node 8)	1.3161	0.1239
WT-2MW (node 10)	1.0712	0.8269
EV-station (node 11)	1.2408	0.1177

the modeling of wind power in correlation with EV are also introduced inspired by similar recent research [47].

Specifically, in Table III, the mean and standard deviation of real power outputs of two WT-2 MW and load of two EV-plug-in-stations in the 14-busbar test system are given. The large deviation around the mean values of wind generation indicates uncertainty in wind availability. On the contrary, there is no large uncertainty in EV load demand/supply. The WT-2 MW at node 7 supply EV-plug-in station at node 8 7018 times out of 15 000 (positive injection of 46.787%). So, the WT-2 MW cannot uninterruptedly supply an expected number of 120 Tesla Roadster plug-in EV. The positive injection is grater than 97.5% if the expected number of Tesla Roadster plug-in EV is lower than 46.79. Consequently, the wind penetration of a WT-2 MW starts to be feebler as the expected number of Tesla Roadster plug-in EV exceeds 47.

To facilitate the correlated modeling of two stochastic profiles, a number of metrics are obviously required. Here, the essentials of them are introduced. Specifically, the wind power penetration into EV-plug-in station is defined as

$$p_{W,EV} = \frac{P_{W,capacity}}{P_{EV,peak}} \tag{27}$$

where $P_{W,capacity}$ is the installed capacity of the wind park and $P_{EV,peak}$ is the peak load demand/supply of the EV-plug-in station.

The energy penetration, which provides a measure of the amount of wind energy produced during a given period compared to the total energy demand/supply of the EV-plug-in station for this period (17), is given by

$$e_{W,EV} = \frac{E_W}{E_{EV,total}}. \tag{28}$$

The correlation of the two profiles is vital as it provides an indication of when the peak of the wind power occurs relative to the load peak demand/supply of EV-plug-in station, given by

$$c_{W,EV} = \frac{\sum_{t=1}^{T} \left(P_W(t) - \overline{P}_W\right) \cdot \left(P_{EV,total}(t) - \overline{P}_{EV}\right)}{(T-1) \cdot \sigma_{P_W} \cdot \sigma_{P_{EV}}} \tag{29}$$

where $P_W(t)$ and $P_{EV,total}(t)$ are the wind power generation and EV-plug-in station load demand/supply at iteration-t, respectively; $\overline{P}_W$ and $\overline{P}_{EV}$ denote the average value of the wind power generation and EV-plug-in station load demand/supply, respectively; σ_{P_W} and $\sigma_{P_{EV}}$ correspond, respectively, to their standard deviations; and T is a given period of each assessed scenario.

Finally, we define the random variable ω, which is the probability of a wind generation and EV demand/supply profile in a certain period (e.g., a day) having a certain correlation coefficient, $c_{W,EV}$ and a certain energy ratio, $e_{W,EV}$. Assuming that $c_{W,EV}$ and $e_{W,EV}$ are independent, the probability of random variable ω is given by

$$f(\omega) = f(c_{W,EV}) \cdot f(e_{W,EV}) \tag{30}$$

whose distribution can be plotted through analysis of databases of wind power and EV demand/supply. Obviously, the larger the databases are, the more accurate the probability distribution of random variable ω is resulted. Since there is no real data base for the correlated integration of wind power with EV demand/supply at the moment, in this study, the probability of random variable ω is plotted from offline databases obtained using (7) for WT-2 MW (node-7) and (16), (17) for EV-plug-in station (node-8).

The probability distributions of energy penetration (28) and correlation factor (29) are plotted in Figs. 4 and 5, respectively. In this analysis, the diurnal EV load and wind power profiles are created by samples of $T = 41$ iterations. So, databases created by 74 825 iterations cover 1825 days (five years). Then, the probability distribution of random variable ω (30) is calculated

TABLE IV
DATA OF THE 14-BUS TEST SYSTEM (IN IEEE FORMAT)

```
11/13/08                    100.0 0    0 FOURTEEN BUS TEST SYSTEM, MODIFIED BY JOHN VLACHOGIANNIS
BUS DATA FOLLOWS                          14 ITEMS
   1 BUS 1    100  1  1  3 1.0100 -16.03    00.00     0.00   230.00    0.00  115.00 1.0200   999.0   -999.0  0.0000  0.0000    0    1
   2 BUS 2    100  1  1  2 1.0000 -15.15    27.61    16.20   120.00    0.00  115.00 1.0000    40.00     0.00  0.0000  0.0000    0    2
   3 BUS 3    100  1  1  0 1.0000 -15.07    77.46    21.00     0.00    0.00  115.00 0.0000     0.00     0.00  0.0000  0.0750    0    3
   4 BUS 4    100  1  1  0 1.0000 -14.79    63.57    -5.03     0.00    0.00  115.00 0.0000     0.00     0.00  0.0000  0.0000    0    4
   5 BUS 5    100  1  1  0 1.0000 -15.10     8.74     1.84     0.00    0.00   15.00 0.0000     0.00     0.00  0.0000  0.0000    0    5
   6 BUS 6    100  1  1  2 1.0000 -14.94     3.22     0.92    10.00    0.00   15.00 1.0000     3.00     0.00  0.0000  0.0000    0    6
   7 BUS 7    100  1  1  2 1.0000 -13.36     0.00     0.00     2.00    0.00   15.00 1.0000    1.800   -1.800  0.0000  0.1500    0    7
   8 BUS 8    100  1  1  0 1.0000 -13.36     1.67     0.00     0.00    0.00   15.00 0.0000     0.00     0.00  0.0000  0.0000    0    8
   9 BUS 9    100  1  1  0 1.0000 -14.94    37.30    21.00     0.00    0.00   15.00 0.0000     0.00     0.00  0.0000  0.0000    0    9
  10 BUS 10   100  1  1  2 1.0000 -15.10     1.70     7.54     2.00    0.00   15.00 1.0000    1.800   -1.800  0.0000  0.1500    0   10
  11 BUS 11   100  1  1  0 1.0000 -14.79     1.68     0.00     0.00    0.00   15.00 0.0000     0.00     0.00  0.0000  0.0000    0   11
  12 BUS 12   100  1  1  0 1.0000 -15.07     7.49     2.01     0.00    0.00   15.00 0.0000     0.00     0.00  0.0000  0.0000    0   12
  13 BUS 13   100  1  1  0 1.0000 -15.15    17.75     7.45     0.00    0.00   15.00 0.0000     0.00     0.00  0.0000  0.0000    0   13
  14 BUS 14   100  1  1  0 1.0000 -16.03    18.74     6.29     0.00    0.00   15.00 0.0000     0.00     0.00  0.0000  0.0600    0   14
-999
BRANCH DATA FOLLOWS                       18 ITEMS
   1    2    1  1 1 0  0.019380  0.059170  0.05280    90   100   110    0 0  0.0000     0.00 0.0000 0.00000.00000  0.0000 0.0000    1
   1    5    1  1 1 0  0.054030  0.223040  0.04920   120   135   150    0 0  0.0000     0.00 0.0000 0.00000.00000  0.0000 0.0000    2
   2    3    1  1 1 0  0.046990  0.197970  0.04380    90   250   305    0 0  0.0000     0.00 0.0000 0.00000.00000  0.0000 0.0000    3
   2    4    1  1 1 0  0.058110  0.176320  0.03740   120   135   150    0 0  0.0000     0.00 0.0000 0.00000.00000  0.0000 0.0000    4
   2    5    1  1 1 0  0.056950  0.173880  0.03400    90   100   110    0 0  0.0000     0.00 0.0000 0.00000.00000  0.0000 0.0000    5
   3    4    1  1 1 0  0.067010  0.171030  0.03460    90   290   310    0 0  0.0000     0.00 0.0000 0.00000.00000  0.0000 0.0000    6
   4    5    1  1 1 0  0.013350  0.042110  0.01280    90   190   210    0 0  0.0000     0.00 0.0000 0.00000.00000  0.0000 0.0000    7
   4    7    1  1 1 1  0.000000  0.209120  0.00000    90   190   210    0 0  0.9780     0.00 0.0000 0.00000.00000  0.0000 0.0000    8
   4    9    1  1 1 1  0.000000  0.556180  0.00000    90   140   180    0 0  0.9690     0.00 0.0000 0.00000.00000  0.0000 0.0000    9
   5    6    1  1 1 1  0.000000  0.252020  0.00000   100   180   190    0 0  0.9320     0.00 0.0000 0.00000.00000  0.0000 0.0000   10
   6   11    1  1 1 0  0.094980  0.198900  0.00000   120   190   200    0 0  0.0000     0.00 0.0000 0.00000.00000  0.0000 0.0000   11
   6   12    1  1 1 0  0.122910  0.255810  0.00000   120   190   200    0 0  0.0000     0.00 0.0000 0.00000.00000  0.0000 0.0000   12
   6   13    1  1 1 0  0.066150  0.130270  0.00000   120   190   200    0 0  0.0000     0.00 0.0000 0.00000.00000  0.0000 0.0000   13
   7    8    1  1 1 0  0.000000  0.176150  0.00000    90   100   110    0 0  0.0000     0.00 0.0000 0.00000.00000  0.0000 0.0000   14
   7    9    1  1 1 0  0.000000  0.110010  0.00000    90   100   110    0 0  0.0000     0.00 0.0000 0.00000.00000  0.0000 0.0000   15
   9   10    1  1 1 0  0.031810  0.084500  0.05000   120   190   200    0 0  0.0000     0.00 0.0000 0.00000.00000  0.0000 0.0000   16
   9   14    1  1 1 0  0.127110  0.270380  0.00000   120   190   200    0 0  0.0000     0.00 0.0000 0.00000.00000  0.0000 0.0000   17
  12   14    1  1 1 0  0.170930  0.348020  0.00000   120   190   200    0 0  0.0000     0.00 0.0000 0.00000.00000  0.0000 0.0000   18
-999
LOSS ZONES FOLLOWS                        0 ITEMS
-99
INTERCHANGE DATA FOLLOWS                  0 ITEMS
-9
TIE LINES FOLLOW                          0 ITEMS
-999
GENERATOR UNIT DATA FOR FOURTEEN BUS TEST SYSTEM
LOAD LEVEL 100
   1    1  1 1      230.0    0.      331.      -999.0    999.0  0.10    10.00
   2    1  1 1      120.0    0.      120.         0.0     40.0  0.10    10.00
   6    1  1 1      10.00    0.       10.         0.0      3.0  0.05     0.50
   7    1  1 1       2.00    0.        2.      -1.800    1.800  0.01     0.10
  10    1  1 1       2.00    0.        2.      -1.800    1.800  0.01     0.10
-999
END OF DATA
```

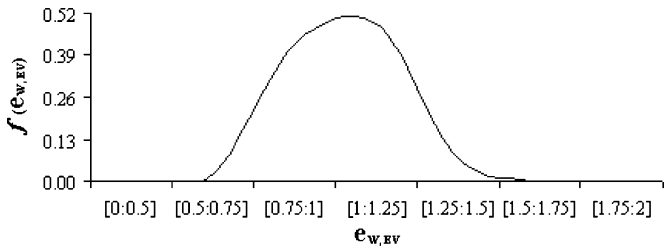

Fig. 4. Probability distribution of wind energy penetration to EV-plug-in station for $p_{W,EV} = 1.2$.

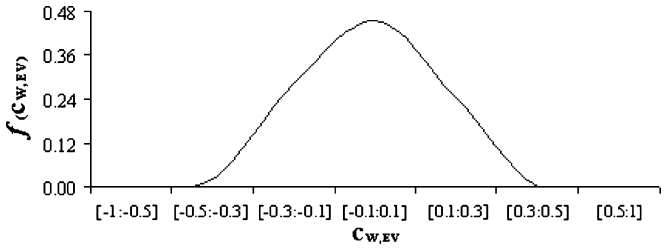

Fig. 5. Probability distribution of the correlation factor between daily wind power and EV demand/supply.

using plotted data of Figs. 4 and 5. The probability distribution of wind energy penetration (Fig. 4) points out that part of the time a WT-2 MW can supply EV-plug-in station with peak load demand of 1.666 MW. The probability distribution plotted in Fig. 5 verifies that the correlation degree of the two stochastic profiles is within the range -0.3 and 0.3. Namely, the two stochastic profiles are slightly correlated, maybe due to the diurnal aspect of the wind resource.

These conclusions are of vital importance for the EV portfolio management. For example, utilities of the system could assign lower prices for EV customers during periods with $e_{W,EV} > 1$ and $c_{W,EV} < -0.3$ (namely, periods with high wind penetration and negative WT-EV stochastic correlation). As a general proposal, utilities should use real-time pricing tariffs which can both smooth-out the diurnal WT generation and EV demand, allowing the last to be increased in response to the availability of costless wind generation. So, holding with similar recent studies [48], the real-time pricing methodology can increase the penetration and utilization of wind power in the system.

Concluding this work, the following originality is set off.

The CLF is modified as a stochastic optimization problem (PCLF) incorporating WT and EV stochastic models. A general EV demand/supply model for load flow studies is developed. The PCLF problem is solved based on stochastic learning techniques using an HLAS. The HLAS comprises new R-CALA useful in this and other power engineering processes. It is demonstrated that R-CALA performance is successful in highly stochastic environment. Its learning methodology improves drastically the HLAS performance despite the wide

range values of control actions. The capability of WT-2 MW to supply specific model of plug-in-EV is analyzed establishing the first benchmark. New formulae useful in correlated integration of two stochastic profiles into the network are introduced and conclusions are drawn for the first time.

As a further work is suggested:

HLAS can be expanded considering more stochastic aspects such as variable grid topologies. HLAS can be slightly modified to be implemented as a multi-agent system (MAS) for the management of new grid architectures. The introduced 14-busbar test system can be further improved taking into account more aspects of modern real power systems. Finally, the developed EV model, new formulation of power flow, and the obtained conclusions in correlated integration of WT with EV into the network can be used in EV portfolio management and market-based power flow control (OPF).

VII. Conclusions

This paper solves the probabilistic constrained load flow by modifying it as an optimization problem considering stochastic models of wind power generation and electric vehicles demand/supply. Therefore, a stochastic model for wind turbine generation is used and a new stochastic model for electric vehicles demand/supply is developed for load flow studies. Due to the hybrid nature of control variables of the probabilistic constrained load flow problem, a hybrid learning automata system is developed comprised by new reward-inaction continuous learning automata. It is implemented to solve the problem on a new 14-busbar test system. The system except conventional components comprises two wind turbine generators and two electric vehicles' plug-in stations. Promised results are gained. New formulae for integration of wind power in correlation with electric vehicles demand/supply into the electricity grids are also introduced resulting in the first benchmark for optimal integration of two stochastic profiles. Crucial conclusions for further studies on electric vehicles portfolio management are drawn.

Appendix

Table IV shows the data of the 14-bus test system (in IEEE format).

Acknowledgment

The author would like to thank the anonymous reviewers for detailed comments on the paper which helped to improve the clarity of the manuscript.

References

[1] W. Kellermann, H. M. Z. El-Din, C. E. Graham, and G. A. Maria, "Optimization of fixed tap transformer settings in bulk electricity systems," *IEEE Trans. Power Syst.*, vol. 9, no. 3, pp. 1126–1132, Aug. 1991.

[2] J. G. Vlachogiannis, "Control adjustments in fast decoupled load flow," *Elect. Power Syst. Res.*, vol. 31, no. 3, pp. 185–194, Dec. 1994.

[3] H. Yoshida, K. Kawata, Y. Fukuyama, S. Takayama, and Y. Nakanishi, "A practical swarm optimization for reactive power and voltage control considering voltage security assessment," *IEEE Trans. Power Syst.*, vol. 15, no. 4, pp. 1232–1239, Nov. 2000.

[4] P. K. Satpathy, D. Das, and P. B. D. Gupta, "A novel fuzzy index for steady state voltage stability analysis and identification of critical busbars," *Elect. Power Syst. Res.*, vol. 63, no. 2, pp. 127–140, Sep. 2002.

[5] B. Cova, N. Losignore, P. Marannino, and M. Montagna, "Contingency constrained optimal reactive power flow procedures for voltage control in planning and operation," *IEEE Trans. Power Syst.*, vol. 10, no. 2, pp. 602–608, May 1995.

[6] E. Vaahedi, Y. Mansour, J. Tamby, W. Li, and D. Sun, "Large scale voltage stability constrained optimal Var planning and voltage stability applications using existing OPF/Optimal VAr planning tools," *IEEE Trans. Power Syst.*, vol. 14, no. 1, pp. 65–74, Feb. 1999.

[7] D. Gan, R. J. Thomas, and R. D. Zimmerman, "Stability constrained optimal power flow," *IEEE Trans. Power Syst.*, vol. 15, no. 2, pp. 535–540, May 2000.

[8] R. A. Jabr and A. H. Coonick, "Homogeneous interior point method for constrained power scheduling," *Proc. Inst. Elect. Eng., Gen., Transm., Distrib.*, vol. 147, no. 4, pp. 239–244, Jul. 2000.

[9] T. S. Karakatsanis and N. D. Hatziargyriou, "Probabilistic constrained load flow based on sensitivity analysis," *IEEE Trans. Power Syst.*, vol. 9, no. 4, pp. 1853–1860, Nov. 1994.

[10] J. G. Vlachogiannis and N. D. Hatziargyriou, "Reinforcement learning for reactive power control," *IEEE Trans. Power Syst.*, vol. 19, no. 3, pp. 1317–1325, Aug. 2004.

[11] J. G. Vlachogiannis, N. D. Hatziargyriou, and K. Y. Lee, "Ant colony system-based algorithm for constrained load flow problem," *IEEE Trans. Power Syst.*, vol. 20, no. 3, pp. 1241–1249, Aug. 2005.

[12] H. Lund and W. Kempton, "Integration of renewable energy into the transport and electricity sectors through V2G," *Energy Pol.*, vol. 36, no. 9, pp. 3578–3587, Sep. 2008.

[13] S. Zoroofi, "Modeling and simulation of vehicular power system," M.Sc. thesis, Chalmers Univ. Technol., Göteborg, Sweden, 2008.

[14] F. Barbir, T. Molter, and L. Dalton, "Regenerative fuel cells for energy storage: Efficiency and weight trade-offs," *IEEE A&E Syst. Mag.*, pp. 35–40, Mar. 2005.

[15] Z. Jiang and R. A. Dougal, "Control design and testing of a novel fuel-cell-powered battery-charging station," in *Proc. 18th Annu. IEEE Applied Power Electronics Conf. Expo. (APEC 03)*, 2003, vol. 2, pp. 1127–1133.

[16] C. C. Chan, "The state of the art of electric and hybrid vehicles," *Proc. IEEE*, vol. 90, no. 2, pp. 247–275, Feb. 2002.

[17] W. Lee, D. Choi, and M. Sunwoo, "Modelling and simulation of vehicle electric power system," *J. Power Sources*, vol. 109, no. 1, pp. 58–66, 2002.

[18] G. T. Heydt, "The impact of electric vehicle deployment on load management strategies," *IEEE Trans. Power App. Syst.*, vol. PAS-102, no. 5, pp. 1253–1259, May 1983.

[19] R. Garcia-Valle and J. G. Vlachogiannis, "Electric vehicle demand model for load flow studies," *Elect. Power Compon. Syst.*, vol. 37, no. 5, pp. 577–582, May 2009.

[20] I. Adan and J. Resing, Queueing Theory, Dept. Math. Comput. Sci., Eindhoven Univ. Technol.. Eindhoven, The Netherlands, 2002. [Online]. Available: http://www.win.tue.nl/~iadan/queueing.pdf.

[21] K. C. Divya and P. S. N. Rao, "Effect of grid voltage and frequency variations on the output of wind generators," *Elect. Power Compon. Syst.*, vol. 36, no. 6, pp. 602–614, Jun. 2008.

[22] K. C. Divya and P. S. N. Rao, "Models for wind turbine generating systems and their application in load flow studies," *Elect. Power Syst. Res.*, vol. 76, no. 9–10, pp. 844–856, 2006.

[23] Y. C. Kim, Y. Sohn, Y. W. Kim, E. C. Lee, I. S. Park, K. R. Kim, K. Gil, C. Chung, J. Y. Ryu, J. I. Park, and C. J. Byun, "Aerodynamic & load calculation for the design of 2 MW wind energy convert system with low speed gearbox," presented at the Eur. Wind Energy Conf. Exhib. (EWEC), Athens, Greece, 2006, paper BL3.153.

[24] V. Akhmatov, *Induction Generators for Wind Power*. Essex, U.K.: Multi-Science, 2007.

[25] T. Lund, P. Sørensen, and J. Eek, "Reactive power capability of a wind turbine with doubly fed induction generator," *Wind Energy*, vol. 10, pp. 379–394, Apr. 2007.

[26] J. Hetzer, D. C. Yu, and K. Bhattarai, "An economic dispatch model incorporating wind power," *IEEE Trans. Energy Convers.*, vol. 23, no. 2, pp. 603–611, Jun. 2008.

[27] R. Viswanathan and K. S. Narendra, "A note on the linear reinforcement scheme for variable structure stochastic automata," *IEEE Trans. Syst., Man, Cybern.*, vol. 2, pp. 292–294, 1972.

[28] B. J. Oommen, G. Raghunath, and B. Kuipers, "Parameter learning from stochastic teachers and stochastic compulsive liars," *IEEE Trans. Syst., Man, Cybern. B, Cybern.*, vol. 36, no. 4, pp. 820–834, 2006.

[29] M. S. Obaidat, G. I. Papadimitriou, and A. S. Pomportsis, "Learning automata: Theory, paradigms and applications," *IEEE Trans. Syst., Man, Cybern. B, Cybern.*, vol. 32, no. 6, pp. 706–709, 2002.

[30] G. I. Papadimitriou, M. Sklira, and A. S. Pomportsis, "A new class of ε-optimal learning automata," *IEEE Trans. Syst., Man, Cybern. B, Cybern.*, vol. 34, no. 1, pp. 246–254, 2004.
[31] G. I. Papadimitriou, A. S. Pomportsis, S. Kiritsi, and E. Talahoupi, "Absorbing stochastic estimator learning automata for S-model stationary environments," *Inf. Sci.*, vol. 147, pp. 193–199, 2002.
[32] B. J. Oommen, S.-W. Kim, M. T. Samuel, and O.-C. Granmo, "A solution to the stochastic point location problem in metalevel nonstationary environment," *IEEE Trans. Syst., Man, Cybern. B, Cybern.*, vol. 38, no. 2, pp. 466–476, 2008.
[33] K. Verbeeck, A. Nowe, P. Vrancx, and M. Peeters, "Multi-automata learning," in *Reinforcement Learning: Theory and Applications*, C. Weber, M. Elshaw, and N. M. Mayer, Eds. Vienna, Austria: I-Tech Education and Publishing, 2008, pp. 167–186.
[34] A. S. Poznyak and K. Najim, *Learning Automata and Stochastic Optimization*, ser. Lecture Notes in Control and Information Science, M. Thoma, Ed. New York: Springer-Verlag, 1997, vol. 225.
[35] N. Baba and Y. Mogami, "A relative reward-strength algorithm for the hierarchical structure learning automata operating in the general nonstationary multiteacher environment," *IEEE Trans. Syst., Man, Cybern. B, Cybern.*, vol. 36, no. 4, pp. 781–794, 2006.
[36] B. H. Lee and K. Y. Lee, "Application of S-model learning automata for multi-objective optimal operation of power systems," *Proc. Inst. Elect. Eng., Gen., Transm., Distrib.*, vol. 152, no. 2, pp. 295–300, 2005.
[37] G. Santharam, P. S. Sastry, and M. A. L. Thathachar, "Continuous action set learning automata for stochastic optimization," *J. Franklin Inst.*, vol. 331, no. 5, pp. 607–628, 1994.
[38] A. Vasilakos and N. H. Loukas, "ANASA—A stochastic reinforcement algorithm for real-valued neural computation," *IEEE Trans. Neural Netw.*, vol. 7, pp. 830–842, 1996.
[39] M. N. Howell, G. P. Frost, T. J. Gordon, and Q. H. Wu, "Continuous action reinforcement learning applied to vehicle suspension control," *Mechatronics*, vol. 7, no. 3, pp. 263–276, 1997.
[40] H. Beigy and M. R. Meybodi, "A new continuous action-set learning automaton for function optimization," *J. Franklin Inst.*, vol. 343, no. 1, pp. 27–47, 2006.
[41] W. Weibull, "A statistical distribution function of wide applicability," *J. Appl. Mech.—Trans. ASME*, vol. 18, no. 3, pp. 293–297, 1951.
[42] D. E. Knuth, *The Art of Computer Programming*. Reading, MA: Addison-Wesley, 1981, vol. II, Seminumerical algorithms.
[43] N. G. Boulaxis, S. A. Papathanasiou, and M. P. Papadopoulos, "Wind turbine effect on the voltage profile of distribution networks," *Renewab. Energy*, vol. 25, pp. 401–415, 2002.
[44] [Online]. Available: http://www.ee.washington.edu/research/pstca/pf14/IEEE14cdf.txt.
[45] [Online]. Available: http://www.teslamotors.com.
[46] H. Banakar, C. Luo, and B. T. Ooi, "Impacts of wind power minute-to-minute variations on power system operation," *IEEE Trans. Power Syst.*, vol. 23, no. 1, pp. 150–160, Feb. 2008.
[47] C. Abbey and G. Joos, "A stochastic optimization approach to rating of energy storage systems in wind-diesel isolated grids," *IEEE Trans. Power Syst.*, vol. 24, no. 1, pp. 418–426, Feb. 2009.
[48] R. Sioshansi and W. Short, "Evaluating the impacts of real-time pricing on the usage of wind generation," *IEEE Trans. Power Syst.*, vol. 24, no. 2, pp. 516–524, May 2009.

John G. Vlachogiannis received the B.Sc. degree in electrical engineering and Ph.D. degree from Aristotle University of Thessaloniki, Thessaloniki, Greece, in 1990 and 1994, respectively.

He is an Associate Professor in the Department of Electrical Engineering of the Technical University of Denmark, Kgs. Lyngby. His research interests include control and management strategies and artificial intelligence techniques in planning and operation of power and industrial systems.

Dr. Vlachogiannis is a member of the Greek Computer Society (Member of *IFIP*, *CEPIS*) and a member of the Technical Chamber of Greece.